Journal of Physics D: Applied Physics

PAPER

Reverse battery model for anodic arc discharges near atmospheric pressure

To cite this article: Carles Corbella *et al* 2019 *J. Phys. D: Appl. Phys.* **52** 485201

IOP Publishing Journal of Physics D: Applied Physics

J. Phys. D: Appl. Phys. **52** (2019) 485201 (13pp) https://doi.org/10.1088/1361-6463/ab3c71

Reverse battery model for anodic arc discharges near atmospheric pressure

Carles Corbella[1], Sabine Portal[1], Madhusudhan N Kundrapu[2] and Michael Keidar[1]

[1] Department of Mechanical and Aerospace Engineering, George Washington University, 800 22nd Street, Northwest, Washington, DC 20052, United States of America
[2] Tech-X Corporation, 5621 Arapahoe Ave. Suite A, Boulder, CO 80303, United States of America

E-mail: ccorberoc@gwu.edu

Received 13 May 2019, revised 2 August 2019
Accepted for publication 19 August 2019
Published 12 September 2019

Abstract

In this study, the macroscopic electrical parameters of anodic arc discharges performed with solid carbon and molybdenum anodes are described in terms of an equivalent circuit. The proposed 1D model shows that the plasma volume behaves as a dissipative medium combined with self-generated voltage from the plasma sheaths. This model is tested by fitting virtual circuits of resistors and batteries to the measured voltage–current (V–I) characteristics representative of atmospheric arc processes (300 and 500 Torr He), resulting in the identification of two phenomena relevant for arc technology. First, steady DC arc experiments show that a minimal arc voltage ($V_0 \approx 20$–30 V) or threshold voltage is necessary to keep the plasma arc on. Second, we prove that pulsed arc discharges excited with rectangular current waveforms (1–5 Hz) are never extinguished but remain ignited during the inactive time of the pulse as long as the aforementioned threshold voltage is maintained. In summary, an atmospheric anodic arc discharge with solid electrodes consumes electrical power as a voltage source opposed to the external voltage supply together with a resistor that accounts for the plasma impedance. This approach permits us to estimate basic plasma parameters from simple electrical diagnostics, as well as to predict how power consumption is distributed within an anodic arc and to understand dynamics of arc plasmas excited by periodic signals.

Keywords: anodic arc discharge, circuit model, atmospheric plasma, pulsed waveform, voltage–current curve

S Supplementary material for this article is available online

(Some figures may appear in colour only in the online journal)

1. Introduction

Anodic arc discharges constitute very efficient sources of nanomaterials because of the high temperatures reached and adjustable technological parameters, such as arc current and working pressure. Among the different nanomaterials, production of carbon nanoparticles like graphene and carbon nanotubes stand out mainly due to their high cristallinity and accurate control of structure and properties [1–4]. A recent example addressing compound material synthesis is the growth of boron nitride nanotubes by arc discharge of boron-based anodes in reactive atmosphere of nitrogen [5]. All the efforts towards control and optimization of arc nanosynthesis require deep understanding of the involved plasma physical processes. In general, tailoring of the extreme structural and functional properties of these materials imply detailed knowledge of the following fundamental steps: (1) Sublimation of the anode to generate gas precursor. (2) Assembly of atoms and molecules in plasma arc to grow nanoparticles. (3) Transport and further growth (agglomeration) of the created particles by diffusion and convection within the chamber. Finally, (4) deposition of the growth flux onto a substrate with adjustable temperature. These processes are currently under investigation from experimental and theoretical approaches, thereby providing up-to-date

recipes of nanomaterial deposition by anodic arc discharges. Usually, the accurate description of such processes either by simulation tasks or analytical approaches is only possible via complex models that couple electrodynamic properties and gas kinetics of the system. The simultaneous consideration of electromagnetic and thermodynamic processes within a multicomponent fluid permits therefore the construction of nanoparticle growth models with increasing accuracy [6].

So far, a number of studies have successfully described plasma dynamics of atmospheric arcs with 1D models in terms of basic electric parameters. In fact, the steady state arc discharge structure is basically composed of the sequence of layers: cathode sheath, arc column and anode sheath [4]. For instance, previous studies have successfully used voltage–current (*V–I*) characteristics measured during arc growth of carbon nanotubes to evaluate plasma parameters like electron temperature, electron density and ion fluxes using a 1D approach [7, 8]. In another study, optical imaging has been correlated to electrical parameters of an equivalent circuit to analyze high pressure sparks [9]. Beyond the established models focused on nanoparticle synthesis, the development of simple models accounting exclusively for electrical properties of arc discharges is still missing. Such new models are very adequate to provide first approximation solutions to the following problems:

1.1. Fast estimation of basic plasma parameters

Balance of energy absorption and power share between arc column and sheaths are very useful data to design more efficient deposition recipes based in arc discharges. Also, the knowledge of such electrical parameters would provide a fast approach to plasma magnitudes like electron density and ionization rates, which otherwise are only accessible by means of standard plasma diagnostics. For instance, Langmuir probe diagnostics constitutes a very efficient but intrusive method of plasma parameter evaluation, since introduction of the electrostatic probe induces modifications in the discharge. Moreover, the obtained data are difficult to interpret in the scenario of large gradients in plasma temperature and density characteristic of atmospheric arc discharges. Optical emission spectroscopy (OES) is a non-invasive, experimentally straightforward technique where the most difficult step is plasma parameter evaluation due to the complexity in optical spectra modelling. In another example, laser techniques such as laser induced fluorescence (LIF) provide reliable data on plasma composition and parameters, but the instrumental preparation is relatively complicated.

1.2. Dynamics of non-stationary, pulsed arc discharges

Such discharges have been recently introduced by Corbella *et al* [10]. Their performance addresses issues of arc instability and powder formation [11–13]. However, the basic mechanisms remain unexplored. For example, the transition from active to inactive phases within a current pulse cycle leads to stable pulsed discharges in a periodic breakdown regime during the whole experiment. Whether such regime implies arc re-ignition or the existence of transient plasma stages is an open question. Such question urges to find an appropriate framework in the form of plasma model. The development and improvement of said model should provide an approximate picture of the basic dynamics of plasma bulk and plasma sheaths in front of periodic variations of arc signals (current and voltage). To the best of our knowledge, a 1D modelling approach of pulsed arc discharges with elementary circuit elements has not been reported yet, in part due to the novelty of such method [10]. All the aforementioned factors justify the convenience of the present study on electrical plasma parameters within the framework of atmospheric arc discharges.

This paper deals with the above issues by proposing a circuit model which mimics the electrical behaviour of anodic arc discharges in helium atmosphere at 300 and 500 Torr. Carbon and molybdenum anodes have been used as example materials. The virtual circuit branch consists of series resistors and voltage sources assigned to plasma column and sheaths, and it is tested by studying arc discharges excited with periodic current signals. The analysis of the respective *V–I* characteristics from signal waveforms provides values of the virtual circuit elements: resistances of the plasma arc and voltage drop at the sheaths are quantified. Finally, the application of this model sheds light onto pulsed arc dynamics and permits to estimate plasma parameters.

2. Experimental details and modelling

2.1. Experimental setup

The anodic arc discharges were performed with an experimental setup described elsewhere [10, 14]. Briefly, the discharges were sustained between two vertically aligned electrodes installed in a cylindrical stainless steel chamber, whose volume is 4500 cm^3. Anode (lower electrode) and cathode (upper electrode) consisted of Poco EDM-3 graphite solid bars with respective diameters of 3 mm and 10 mm. A molybdenum anode (99.95%) with 3 mm in diameter was also used. The inter-electrode gap during arc discharge was comprised between 0 and 12 mm. Cathode position was fixed and anode vertical position was regulated through a computer-controlled stepper motor. The vessel was continuously pumped by means of a mechanical pump down to a background pressure lower than 0.1 Torr. The system was fed with helium gas (99.995%) up to 500 Torr through an electro valve gas input. The working pressure was adjusted at the gas output by means of a manual throttle valve. The electrodes were connected to the terminals of a Miller Gold Star 300SS DC power supply, which was used to ignite and support the arc discharge. Details regarding source operation can be found in the supporting information file (stacks.iop.org/JPhysD/52/485201/mmedia). Initially, the powered electrodes are brought in contact and short-circuited. The discharge strikes upon separation of the electrodes. The power supply was current-regulated and remotely controlled by a waveform generator. The supplied current was proportional to the waveform voltage amplitude within a range from 0 through 5 V. Hence, the maximal value of stable arc current was approximately 150 A, whereas peak arc current was

limited to around 250 A. Figure 1 shows the basic electrode configuration together with the two periodic waveform signals used in this study: rectangular pulse signal (1, 2 and 5 Hz with nominal edge time of 5 ns) and symmetric triangular signal (1 and 2 Hz). All electric measurements were performed with a 4-channel oscilloscope and a calibrated current clamp. Arc discharge processes were recorded by a digital camera (≈10 frames s^{-1}) through a glass port view protected with a strongly absorbing filter.

2.2. Modelling

Here, the arc discharge is described through a simple 1D model. The treated region consists of the arc space comprised between anode and cathode. It corresponds to the arc length, so the considered parameters depend only on such length. Figure 2 shows a schematic representation of potential distribution of the arc discharge within the inter-electrode gap. This sketch is accompanied with the proposed equivalent circuit model for the arc discharge. The plasma arc can be depicted as a series circuit with active and passive elements. The passive element of the circuit consists of a plasma arc resistance, R_{arc}, which is equal to the sum of cathode sheath resistance, $R_{s,c}$, anode sheath resistance, $R_{s,a}$, and plasma column resistance, R_{col}. Mathematical expression: $R_{arc} = R_{s,c} + R_{s,a} + R_{col}$. This component is connected in series to a voltage source, which is the active element of the circuit and whose voltage is the sum of voltage drops generated at cathode sheath, $\varepsilon_{s,c}$, and at anode sheath, $\varepsilon_{s,a}$. In other words: $\varepsilon_s = \varepsilon_{s,c} + \varepsilon_{s,a}$. In this approach, the total voltage drop across the inter-electrode gap, arc voltage V_{arc}, is generated by the response of the plasma resistance and of the sheath voltage source to the arc current, I_{arc}. The following general expression applies to this scenario:

$$V_{arc} = \varepsilon_s + R_{arc} \times I_{arc}. \quad (1)$$

The voltage source provides a constant voltage that opposes to the external current supply. Thus, arc current flows from anode to cathode only when $V_{arc} \geqslant \varepsilon_s$. Otherwise, there is no arc current and the plasma vanishes. In this model, ionic and electronic contributions are not distinguished in the total current in the plasma arc. The sheath voltage source defines a threshold for the arc voltage so that plasma can be sustained. The electrical measurements in this study will be discussed within the context of this model. Roughly, plasma arc behaves as a purely dissipative medium with an opposed voltage source, similar to a battery with internal resistance R_{arc}. To keep a simple notation, we refer to the constant voltage drop from sheaths as $V_0 \equiv \varepsilon_s$. The objective of this study is to evaluate R_{arc} and V_0 in steady and pulsed arc discharges, and to discuss their correlation with basic plasma parameters.

3. Results

3.1. DC arc discharges: study of plasma column

The voltage drop of carbon anodic arcs at the plasma column, V_{col}, has been obtained from the temporal evolution of the arc voltage at constant arc current. V_{arc} is expected to increase linearly with time for a constant ablation rate. It is assumed that the plasma column elongation is equal to the gap separation, since sheath thicknesses are of the order of micrometer [16]. The experiments were performed at 300 Torr and 500 Torr He with arc currents of 60 A and 150 A flowing between the electrodes. Figure 3 shows the curves corresponding to 300 Torr experiments. The linear fit on the plots of arc voltage versus gap separation provides V_{col} and the sheath voltage, V_s, as indicated in the example. For a given discharge, the total plasma voltage drop can be expressed as $V_{arc} = V_s + V_{col}$, where V_s is considered constant because the sheath potential drops are practically unaffected by the gap length [17]. The data taken at small distances deviates from linearity, which is a known issue in very narrow gaps due to coupling between anode and cathode sheath regions [7, 18]. Therefore, such points were not considered in the linear fittings. Another reason of the initially non-linear behaviour of arc voltage may be introduced by electrical conductivity decrease of the electrodes due to melting process. This effect is assumed to exert a low impact on arc column resistance because changes in electrode conductivity are absorbed into the values of sheath resistances R_s discussed in section 3.2. Electrical resistance associated to the plasma column is evaluated as $R_{col} = V_{col}/I_{arc}$. This resistance achieved maximal values between 0.01 Ω and 0.10 Ω in the present experiments. In a further step, the electrical conductivity of the plasma column, σ, has been determined from the slope of the fitted curve according to the expression:

$$\sigma = \frac{x}{R_{col}} \frac{1}{S} \quad (2)$$

where x is the gap separation and S is the plasma column section. In this case, S has been calculated approximating a column diameter equal to the anode diameter, i.e. 3 mm, because it is the size of the deposit on cathode surface (see image in figure 1). The gap separation was deduced from the anode length variation after each process, which matched well with the ablation rates ≈2 mg s^{-1} at $I_{arc} = 60$ A, and ≈20 mg s^{-1} at $I_{arc} = 150$ A. Such ablation rates match with the values reported in our previous study [10]. The values of σ at 60 A and 150 A in arc current were 1–3 × 10^4 S m^{-1} and 1–2 × 10^5 S m^{-1}, respectively (see table 1). The electrical conductivity in DC plasmas is proportional to electron density, n_e, from the expression [19]:

$$\sigma = \frac{e^2 n_e}{m_e \nu_m}. \quad (3)$$

Here, m_e is the electron mass, e is the elementary charge, and ν_m is the electron-neutral collision frequency. This last variable adopted values within the range 10^9–10^{10} s^{-1} according to the equation $\nu_m = n_g s \langle v_e \rangle$, where n_g is the neutral gas density calculable from ideal gas equation; s is the collision cross section, which is approximately 10^{-16} cm^2 [16], and $\langle v_e \rangle$ is the average thermal electron velocity from a classical electron gas with an electron temperature $T_e \approx 1$ eV. The respective estimates of n_e at 60 A and 150 A are $n_e \approx 2$–3×10^{21} m^{-3} and $n_e \approx 3 \times 10^{22}$ m^{-3}, which agree well with results from arc discharge simulations [20].

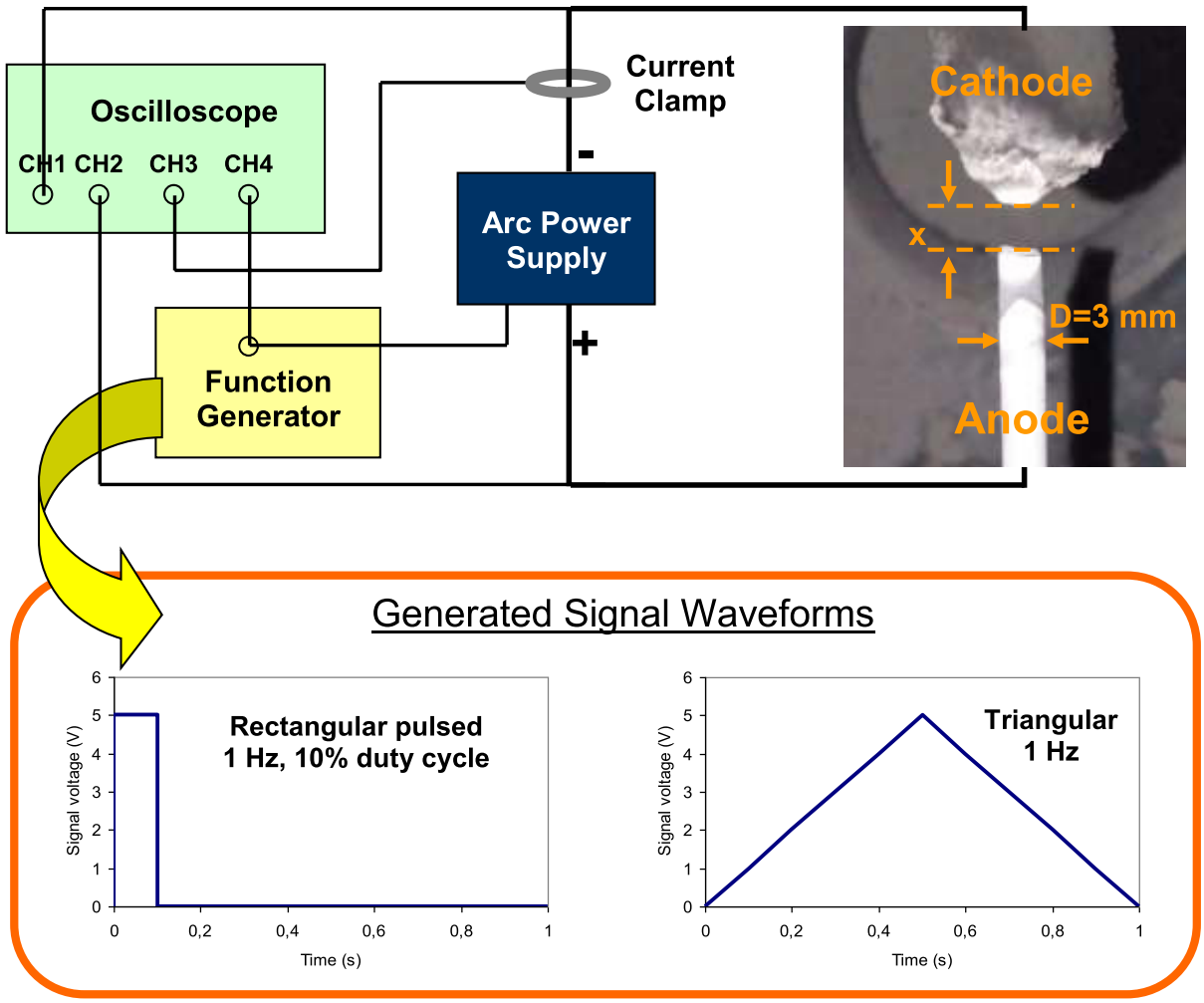

Figure 1. Configuration of anode and cathode inside the plasma arc chamber together with a sketch of the measurement setup. Anode diameter ($D = 3$ mm) and range of inter-electrode gap ($x = 0$–12 mm) are indicated. The current-regulated power supply is operated in remote mode by means of a waveform generator. Examples of the generated waveform signals used in this study (pulsed and symmetric triangular) are depicted. The following signals are measured by means of an oscilloscope: CH1 = cathode voltage; CH2 = anode voltage (CH2–CH1 = discharge voltage); CH3 = discharge current; CH4 = pulse signal waveform (figure adapted from [10]). Thicker connecting lines represent high power cables attached to the arc power source.

Similarly, the voltage drop corresponding to Mo arc discharge has been studied by analyzing the arc voltage variation with inter-electrode distance at 300 Torr (figure 4). In this case, a Mo anode of 3 mm in diameter and a graphite cathode of 10 mm in diameter have been used. The reason of using carbon as cathode lies in the relatively high melting temperature of carbon (around 4000 K) compared to molybdenum melting point (2900 K). Carbon was thereby chosen as cathode material to avoid issues associated to melting and, therefore, to achieve a stable arc discharge thanks to stable thermionic emission of the hot cathode. Similar strategy of using refractory materials as cathode was followed in a recent study [5]. However, the Mo anode melted already at very low arc currents, so an experiment with DC arc discharge sustained uniquely at 30 A was performed. Figure 4(a) shows that the arc parameters were not stable with time. Such variations are attributed to anode melting occurring simultaneously to ablation. Indeed, the progressive anode melting hinders arc stability. Figure 4(b) shows the drop with melted material formed on top of a Mo anode after DC arc discharge. The ablation rate was $\approx$1.5 mg s^{-1}, whereas anode melting was significant: the melted-to-ablated mass ratio is around 150. The voltage drop curve yields values of $\sigma = 2000$ S m^{-1} and $n_e = 3 \times 10^{20}$ m^{-3} as calculated with equations (2) and (3). These values suggest that Mo anodic arc provides lower plasma density than carbon arc discharge, probably due to the low arc current supplied.

3.2. DC arc discharges: study of plasma sheaths

The calculations above provided information on the electrical properties of the plasma column, and now we will focus on the electrical parameters of plasma sheaths of DC arc discharges. Voltage drop at the plasma sheaths, $V_s = V_{s,c} + V_{s,a}$, is generated by the combined effect of the sheath resistances, $R_s = R_{s,c} + R_{s,a}$, and of the minimal sheath voltage, $\varepsilon_s = \varepsilon_{s,c} + \varepsilon_{s,a} = V_0$. Then:

$$V_s = V_0 + R_s \times I_{arc}. \quad (4)$$

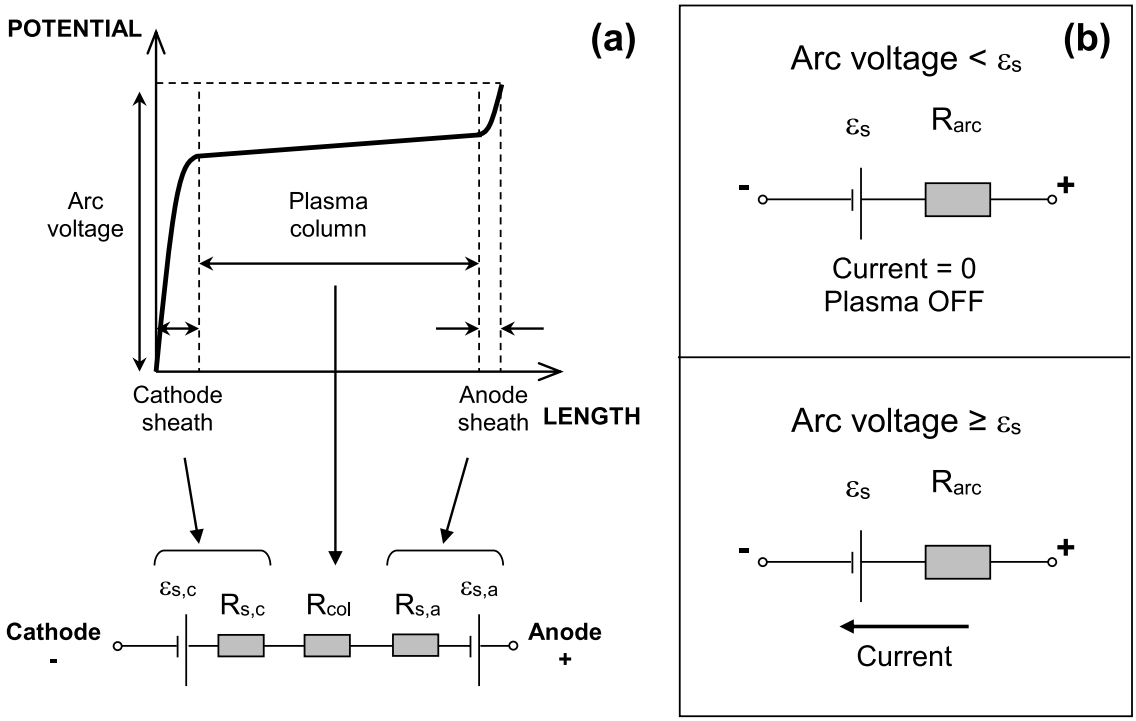

Figure 2. (a) 1D sketch of potential distribution along plasma arc together with equivalent circuit model. A negative anode sheath (electric field towards anode) is also possible if arc is constricted at the anode (see section 4) [15]. Anodic arc discharge is modelled as a series association of virtual resistors and batteries. (b) Compact sketch of the series circuit in the situations where arc voltage is lower (top) and higher (bottom) than the sheath voltage source. $R_{arc} = R_{s,c} + R_{s,a} + R_{col}$; $\varepsilon_s = \varepsilon_{s,c} + \varepsilon_{s,a} \equiv V_0$.

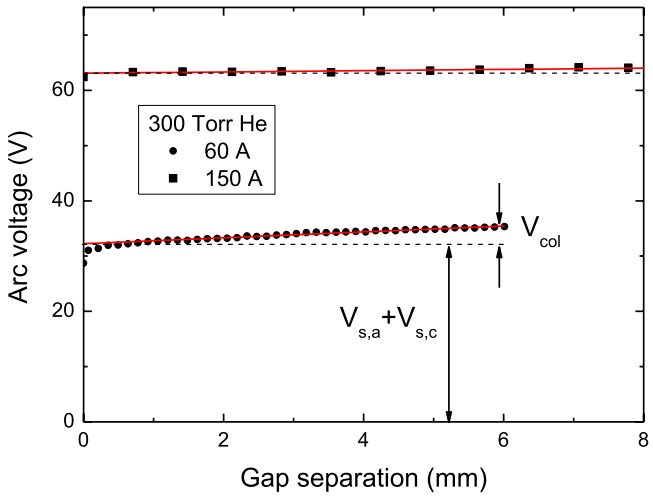

Figure 3. Evolution of arc voltage in DC arc discharges sustained between graphite electrodes at 60 A and 150 A for a working pressure of 300 Torr. The curves at 500 Torr show similar behaviours. The determination of plasma column voltage, V_{col}, and of sheath voltages, $V_s = V_{s,c} + V_{s,a}$, is illustrated for the arc discharge at 60 A.

To determine such parameters, we need to study the variation of arc voltage with respect to arc current, i.e. to analyze the *V–I* characteristics of the arc discharge. These curves were obtained as follows. Arc discharges were sustained with variable arc currents following periodic triangular waveforms at 1 Hz and 2 Hz during several cycles. The selected frequency had no influence on the shape of the obtained waveforms. Figure 5 shows examples of current and voltage waveforms applied to arc discharges at 300 Torr and 500 Torr with carbon electrodes. Mo arc discharges show arc instabilities due to melting issues. Thus, Mo arcs operated with variable current were not analyzed. Initially, the energized electrodes are short-circuited, so voltage is proportional to current according to Ohm's law. The proportionality constant is the value of contact resistance. As soon as a gap is formed between the electrodes, the arc discharge strikes and the voltage waveform is shifted to higher values. In parallel, the maximal values of the current waveform are slightly reduced. Another feature during arc operation is the asymmetry on voltage waveform within one cycle: arc voltage is more noisy at decreasing voltages. The origin of the observed voltage spikes might be ascribed to arc instabilities due to rarefaction of the hot gas and projection of droplets from the ablating anode. Voltage-to-current ratios are also represented on figure 5. Please note that the arc voltage is measured at the electrical contacts of anode and cathode outside of the arc chamber. Therefore, the ratio depicted between points I and II (short-circuited electrodes) accounts for the sum of series contact resistances located between the voltage measuring points. Furthermore, the ratio from point II to point III (arc plasma) shows minimal values at the peak values of current and diverges when there is no current flowing. The relation between voltage and current at the plasma region requires further analysis which will be performed below.

Importantly, it must be proved that current and voltage waveforms shown in figure 5 were obtained in steady DC arc conditions. This question is addressed by analyzing the optical emission of graphite anode during one current cycle at 1 Hz and 300 Torr (figure 5(a)). The sequence of images shown in

Table 1. Electrical parameters determined for DC and pulsed anodic arc discharges with carbon and molybdenum electrodes. The basic parameters of the model are V_0, R_s and R_{col}. They have been obtained by fitting the model (equations (1), (2) and (4)) to the experimental data after two experiments at least. Thus, arc voltage can be represented as a function of current and arc length as predicted by the proposed model. Please note that $R_{arc} = R_s + R_{col}$ and that R_s for pulsed arcs correspond to the stable values. The plasma conductivity values, σ, are correlated to R_{col} and to n_e values through equations (2) and (3), respectively. Power dissipated by Joule effect: $P = R \times I^2$.

	Mo DC arc (300 Torr)	Carbon DC arc (300 and 500 Torr)		Carbon pulsed arc (300 Torr)	
	30 A	60 A	150 A	1 Hz, 2 Hz max 250A	5 Hz
Ablation rate (mg s^{-1})	1.5	2–3	20	10/pulse	10/pulse
Threshold voltage, V_0 (V)	≈20	25–30	25–30	15–25	15–25
Sheath resistance, R_s (Ω)	—	0.12–0.16	0.12–0.16	0.11–0.14	—
Column resistance, R_{col} (Ω)	≈1	0.01–0.10	≈0.01	<0.01	<0.01
Plasma resistance, R_{arc} (Ω)	—	0.13–0.26	0.12–0.16	0.11–0.14	—
Electrical conduct., σ (S m^{-1})	2×10^3	$1–3 \times 10^4$	$1–2 \times 10^5$	$>2 \times 10^5$	—
Electron density, n_e (m^{-3})	3×10^{20}	$2–3 \times 10^{21}$	3×10^{22}	$>3 \times 10^{22}$	$>3 \times 10^{22}$
Sheath power share, R_s/R_{arc}	—	>50%	>90%	>90%	—
Col. power share, R_{col}/R_{arc}	—	5%–50%	<10%	<10%	—

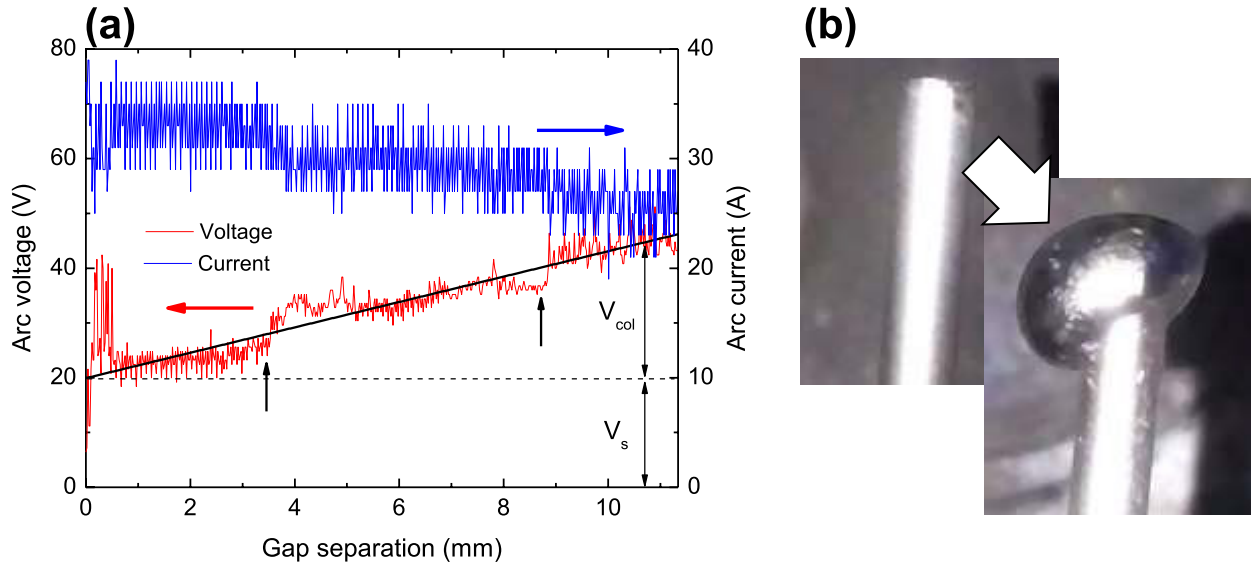

Figure 4. (a) Evolution of arc voltage and arc current in DC arc discharges sustained between graphite cathode and ablating Mo anode at an average current of 30 A for a working pressure of 300 Torr. The determination of plasma column voltage, V_{col}, and of sheath voltages, $V_s = V_{s,c} + V_{s,a}$, is illustrated. Linear fitting of arc voltage curve is indicated with a black solid line. The arc instability regions highlighted with vertical arrows are associated to shape modification of the anode due to melting. (b) Images of the Mo anode before and after the arcing process, which lasted a total time of 7 s. Mo anode diameter: 3 mm.

figure 6, which were captured with 0.12 s of time interval, shows that the optical emission pattern corresponds to steady DC anodic arc discharge. As reported elsewhere, this pattern is characterized by a predominant light emission coming from the anode tip, in contrast with plasma glow located between both electrodes characteristic of non-stationary pulsed arcs [10]. The arc diameter ratio related to optical emissions taken at $I_{arc} \approx 100$ A and $I_{arc} \approx 200$ A, D_{200}/D_{100}, is approximately 2. This suggests that current density increases with arc increase. The fact that arc radius is roughly proportional to arc current at high current values is a typical signature of anodic arc [8]. In conclusion, the observed optical emission patterns support the hypothesis of arc discharge operation in stationary, steady DC mode. Most importantly, although the discharge burns with variable intensity depending on the phase of the cycle, the discharge remains ignited in DC regime during the whole process since the pattern of arc breakdown discharge (core located at the intermediate position between electrodes) is never observed in these experiments [10].

The waveform data plotted in figure 5 are represented as *V–I* curves in figure 7, where one can observe two well-distinguished behaviours. It is worth noting the transition from the initial linear, Ohmic behaviour during the short-circuit phase to the particular relation between current and voltage upon arc ignition. The reproducibility of the *V–I* curves of several plasma cycles agrees with the fact that the arc discharge is not extinguished during the triangular cycles, but it remains ignited. The plasma characteristics are similar to the short-circuit characteristics but they are floating above a potential V_0 and are more noisy (especially at 500 Torr). In other words, *V–I*

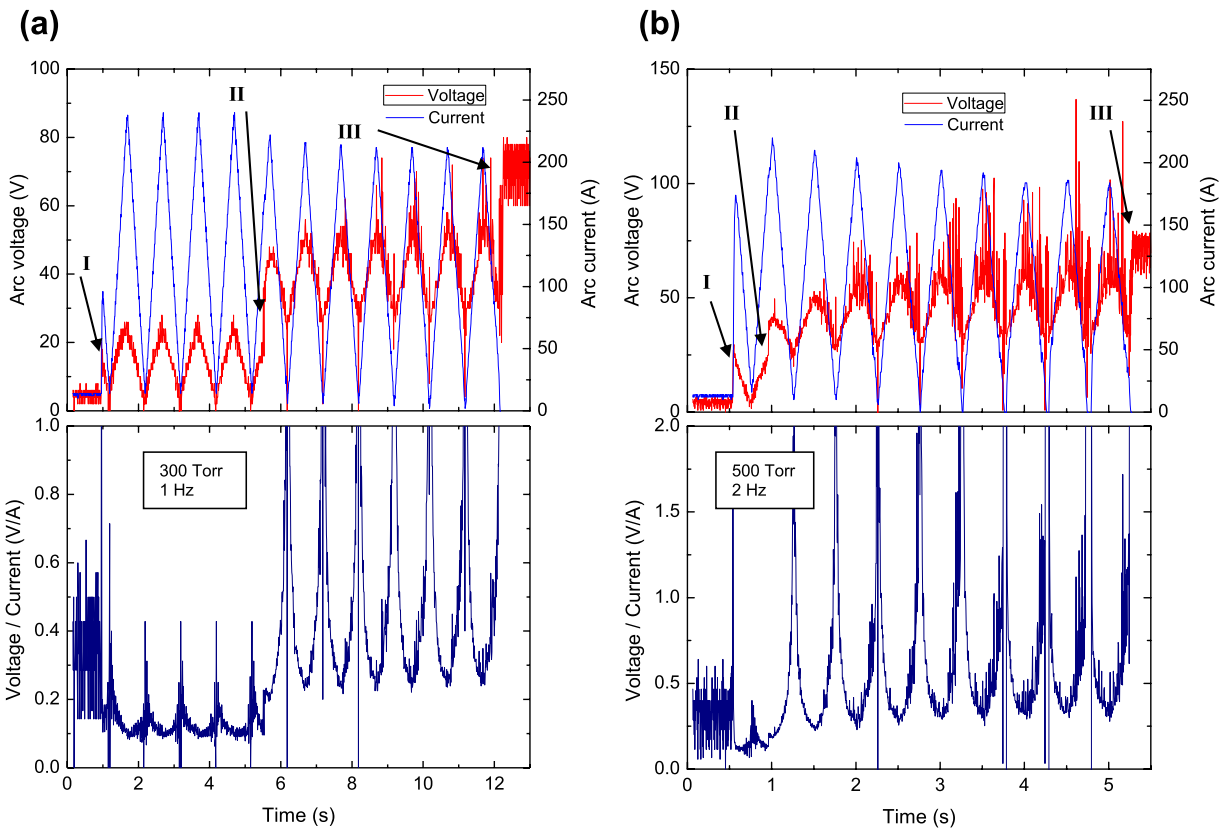

Figure 5. *Upper plots*: current and voltage waveforms as response to symmetric triangular excitation signal applied to graphite electrodes at (a) 1 Hz for 300 Torr and (b) 2 Hz for 500 Torr. *Lower plots*: corresponding temporal evolutions of *V*-to-*I* ratios. Point I: contacting (short-circuited) electrodes are powered; point II: plasma strikes as electrodes are separated; point III: plasma is extinguished.

characteristics of arc plasmas show a linear evolution shifted to a higher constant voltage value. This behaviour contrasts with the result found by Shashurin *et al* [7], where *V–I* curves showed non-linear evolution (V-type shape). Nevertheless, this earlier paper reports arc discharges on carbon hollow anodes full of metal catalyst for nanotube growth applications, while in the present study we are dealing with solid anodes. If we neglect the voltage drop at the plasma column, i.e. $V_{\mathrm{col}} \ll V_{\mathrm{s}}$, the represented arc voltage can be approximated to the voltage drop at the sheaths, $V_{\mathrm{arc}} \approx V_{\mathrm{s,c}} + V_{\mathrm{s,a}}$. The potential V_0 is assumed to be the voltage supplied by the sheaths, $V_0 = \varepsilon_{\mathrm{s}}$, which defines a zero-current threshold to sustain the plasma. The discharge extinguishes if the arc voltage is lower than V_0, which eventually happens as displayed in figure 5 (point III).

The electric parameters that define the equivalent circuit (model in figure 2) are quantified from the linear fit analyses on the plots of arc voltage, V_{arc}, on figure 7. The linear fits were performed only on the increasing voltage branches of three stable cycles at each pressure. Thus, sheath resistance, R_{s}, and the threshold voltage, V_0, are provided according to equation (4) by identifying $V_{\mathrm{arc}} = V_{\mathrm{s}}$ ($V_{\mathrm{col}} \ll V_{\mathrm{s}}$) and $V_0 = \varepsilon_{\mathrm{s}}$. Sheath resistances of the order of 0.15 Ω and threshold voltages of around 25–30 V have been obtained from this analysis. eV_0 is consistently higher than the first ionization energy of carbon (11.3 eV). The detailed results are summarized in table 1.

3.3. Application to pulsed arc discharges

As recently introduced, pulsed arc discharges with ablating carbon anode show adequate performance in nanoparticle synthesis at the frequency range 1–5 Hz [10]. Here, we analyze the pulsed current and voltage waveforms to obtain the electrical parameters of pulsed arc discharges at 1, 2 and 5 Hz. Figure 8 shows three representative waveforms together with optical emission images captured at the instant of maximal plasma emission within a pulse cycle. The waveforms can be divided into three regions, namely *region i*, or region previous to the current and voltage increase; *region ii*, or region during active part of the pulse (plateau); and *region iii*, or region posterior to decrease of signals. Regions *i* and *iii* correspond to the inactive part of the pulse, and they are usually stabilized on a positive voltage. Region *ii* shows the maximal voltage and current associated to the arc after a short rise time. The transient response time of arc current will be discussed later. Moreover, the recorded signals are distorted by higher frequency harmonics: the frequency spectra of the pulse signals depicted in the supporting information show the presence of 60 Hz-harmonics generated by the electric network system.

The electrical properties of pulsed arc discharges are to be studied within the context of *V–I* curves. For this, voltage values have been plotted against current values in pulsed discharges in two distinct situations: before separation of electrodes, when they are short-circuited; and after their

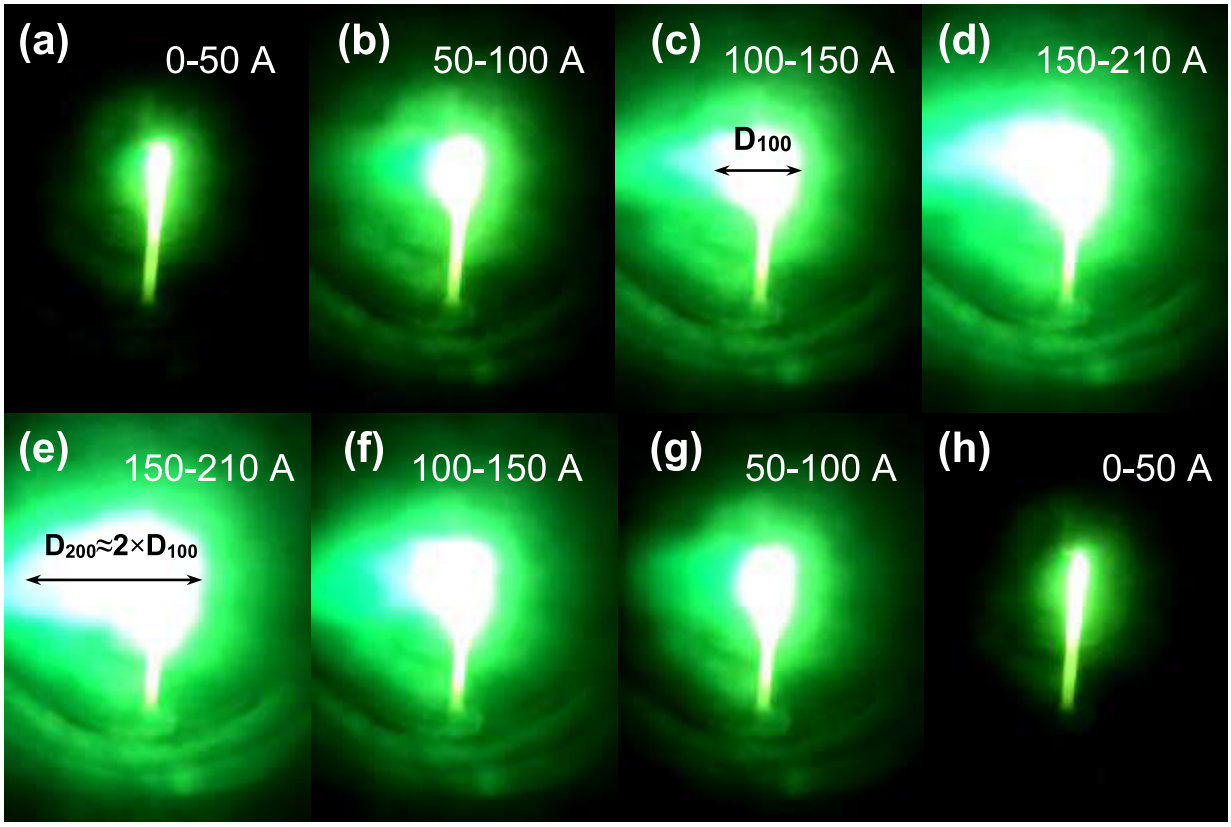

Figure 6. Pictures of the arc discharge taken every 0.12 s during triangular signal excitation applied to graphite electrodes at 1 Hz and 300 Torr. The arc current intervals are indicated. Images (d) and (e) show the characteristic emission at around 200 A, whereas images (a) and (h) correspond to low arc currents. The arc diameter (or size) ratio D_{200}/D_{100} is approximately 2, thereby suggesting proportionality between arc diameter and arc current at high current values.

separation, when plasma arc is ignited. Figure 9 shows these two scenarios by means of the representative *V–I* characteristics of one pulse cycle in the two situations described above. Both curves evidence a hysteresis within one period due to a phase-shift between arc voltage and current. In particular, *V–I* curve in short-circuit shows a smoothly increasing trend as the pulse starts (region *i*); the system remains for some time in the plateau (region *ii*), and it returns to zero volts as the pulse finishes (region *iii*). The *V–I* curve in arc discharge conditions shows a different pattern: while the shape of the curve is slightly distorted but it does not undergo any substantial change, the whole characteristic is shifted to a higher voltage value. This result coincides qualitatively with the behaviour displayed above by arc electrodes when they are energized with DC power (figure 7), where the most visual effect of plasma striking is the application of a voltage offset to the original *V–I* characteristics.

Figure 10 shows the *V–I* characteristics corresponding to the waveforms displayed in figure 8. The basic structure of hysteresis is the same for the three explored frequencies. In all cases, the characteristics float above the threshold voltage, V_0, which is used as reference to evaluate the plasma resistances. The extreme points *i*, *ii* and *iii* account for the initial, saturation and final position within the waveforms, respectively (figure 8). Plasma resistance is calculated using equation (1), which is representative of the equivalent circuit. A distinctive feature of pulsed arcs is that they exhibit a plasma resistance that changes with time, thereby manifesting the non-stationary nature of pulsed discharges. The stable value of plasma resistance, R_{arc}, is approximated to 0.11–0.14 Ω for 1 Hz and 2 Hz, whereas no stable regime was achieved at 5 Hz. In pulsed arcs, the plasma column resistance is very difficult to determine because the plasma structure changes periodically, which makes the monitoring of potential variation challenging. Therefore, plasma electrical conductivity and/or electron density should be measured with plasma diagnostics such as OES. Nevertheless, one can assume a lower estimate of $n_e \approx 3 \times 10^{22}$ m^{-3} at the maximal current phase (region *ii*). Such electron density was determined for the 150 A-DC arc discharge, and it is plausible to assume that plasma density achieves higher values in the 250 A-plateau region of the pulse. Concerning threshold voltage, V_0 was comprised between 15 V and 25 V. Similar to the case of DC arc discharge, signal becomes noisy in the receding part of the pulse, where voltage spikes account for arc instabilities when arc current decreases. Instabilities at 1 Hz usually eliminate the threshold voltage V_0 due to the long inactive time compared to 2 Hz- and 5 Hz-processes, which causes important modification in the discharge structure and may end up extinguishing the discharge.

The persistent hysteretic behaviour observed in *V–I* curves is caused by the participation of an additional electrical component that causes a phase-shift to appear between current and voltage. The transient response time observed in current

pulses may be introduced by the equivalent inductance from the transformer coils built in the DC power supply (see supporting information). The overall stray inductance, L_{stray}, can be evaluated by measuring the rise time or decay time of the arc current within a pulse cycle, τ, which is of the order of 10 ms. According to the approximation $\tau = L_{stray}/R_{DC}$, and knowing the internal resistance of the DC power supply $R_{DC} = 12\ \Omega$, one obtains $L_{stray} = 120$ mH. Please note that such inductance value is not expected to modify the triangular waveforms at 1 or 2 Hz. Consistently, the respective *V–I* curves do not show hysteresis (figure 7).

4. Discussion

This section aims to summarize the results from the above reported experiments and to discuss some implications of the proposed model. Especially, emphasis is put on the separation of total current into electronic and ionic contributions, and on the description of the different discharge phases observed during pulsed anodic arc discharges of carbon electrodes.

4.1. Arc plasma parameters

Table 1 lists the resistance and threshold voltage values measured in every arc discharge condition. Moreover, ranges of power share in sheath and arc column regions are indicated. Table 1 clearly shows that most of input power is consumed at the level of plasma sheaths. Such effect is more pronounced at high arc current, mainly owing to the significant increase in conductivity of the arc column. It is worth noting that the evaporation dynamics of Mo anode differs substantially from that found in graphite anode due basically to the melting issue. This point certainly deserves a separate study in the future considering the impact of the molten electrode on the circuit model parameters due to changes in anode shape, temperature and electrical resistances.

Although the circuit model does not distinguish between electronic current, I_e, and ionic current, I_i, here we discuss the possible values of these parameters. Expressions for electronic and ionic contributions to total current at the carbon cathode are shown in equations (5) and (6), so that $I_{arc} = I_e + I_i$. Electronic current is taken from the Richardson's equation for thermionic current. On the other hand, ionic current has been calculated based on the Bohm condition at cathode sheath-edge assuming that the cathode sheath is collisionless [8, 16].

$$I_e = \pi r_C^2 A T_C^2 \exp\left(-\frac{\varphi_W}{\kappa T_C}\right) \quad (5)$$

$$I_i = \pi r_A^2 0.6 e n_e \left(\frac{\kappa T_e}{M_i}\right)^{1/2}. \quad (6)$$

In these expressions, T_C is the cathode temperature, κ is the Boltzmann constant, and M_i is the ion mass (12 u for carbon and 95.9 u for molybdenum anodic arcs). The radii of electron and ion beams at cathode surface are, respectively, $r_C = 5$ mm (cathode radius) and $r_A = 1.5$ mm (anode radius). Here, we assigned r_A to ion beam spot at cathode because the deposit

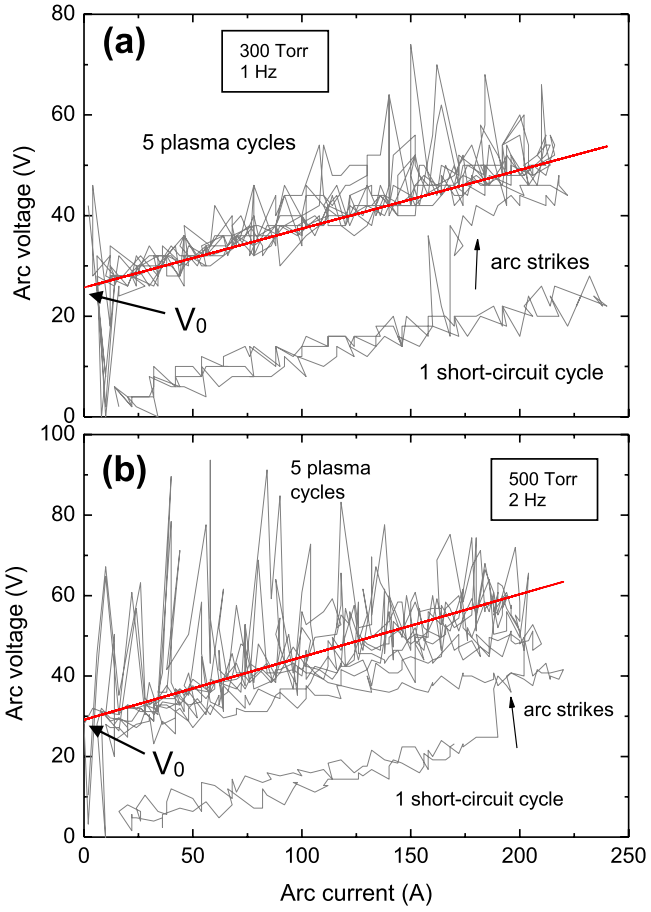

Figure 7. *V–I* characteristics of DC arc discharges excited with symmetric triangular signal applied to graphite electrodes at (a) 300 Torr and 1 Hz, and (b) 500 Torr and 2 Hz. Linear fit analyses on the plots of arc voltage, V_{arc}, which are represented with red straight lines, provided the sheath resistance, R_s (slope), and the threshold voltage, V_0 (intercept).

on cathode surface shows a circular shape with radius $\approx r_A$. Electron temperature has been taken $T_e \approx 1$ eV, and the electron density values, n_e, are extracted from table 1. The constant in the Richardson's equation for thermionic electron current (equation (5)) is $A = 120\ \mathrm{A\ cm^{-2}\ K^{-2}}$. The work function of the carbon cathode is $\varphi_W = 4.62$ eV, although it can be slightly modified during arc due to material deposition [21]. Figure 11 shows an example on how cathode temperature T_C is determined from the values of I_i, I_e and set total current, I_{arc}. There, arc current curve is computed from I_i and I_e curves, and it is plotted against cathode temperature in order to evaluate T_C that best fits to the set total current.

Table 2 summarizes data corresponding to electronic and ionic currents from the arc discharges analyzed here. The electronic current dominates in all cases, which contrasts with the output from the model by Keidar and Beilis [8], where higher ion fractions were evaluated. However, it is difficult to establish a direct comparison since the earlier study considered hollow carbon anodes filled with metal catalyst aimed to nanotube growth, while here we consider merely solid anodes. The range of cathode temperatures matches with the simulation values by Keidar and Beilis [8] and with *in situ* measurements by Yeh *et al* [22]. The ionization degree of the vaporized

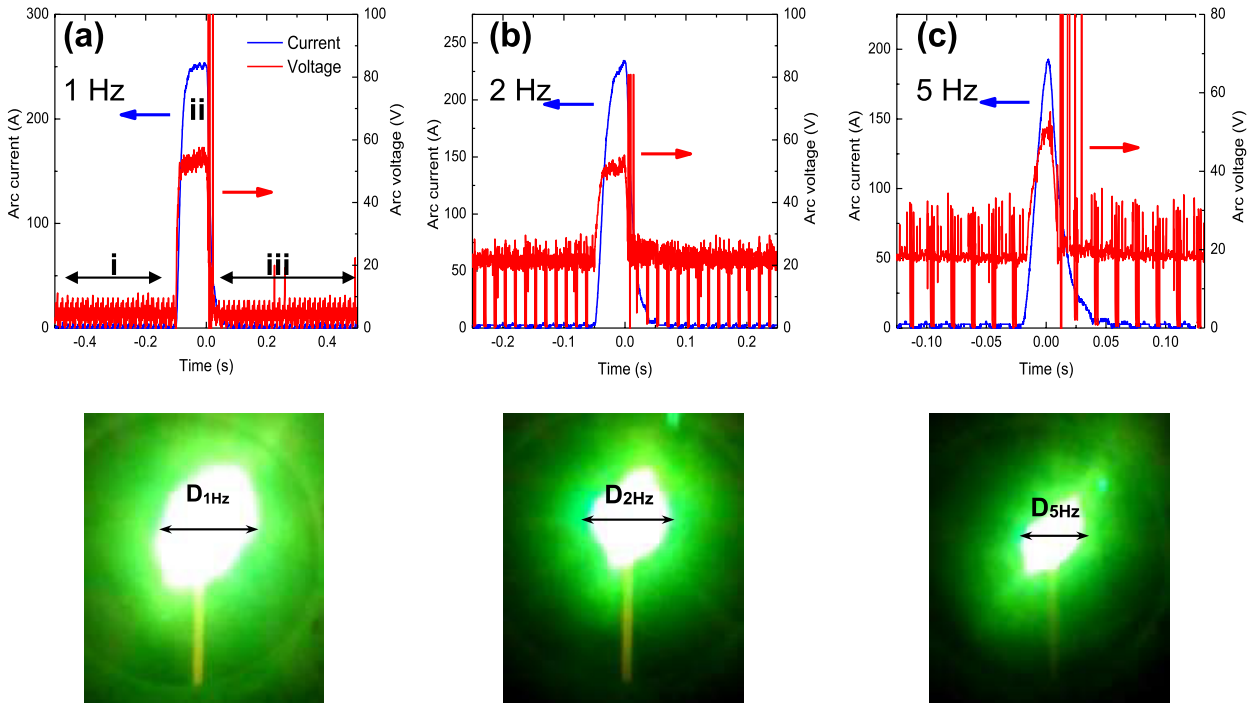

Figure 8. Current and voltage waveforms corresponding to pulsed arc discharges with carbon anode held at (a) 1 Hz, (b) 2 Hz and (c) 5 Hz at 300 Torr. Regions *i*, *ii* and *iii* will be discussed in *V–I* characteristics (see figure 9). The bottom figures show images of the corresponding pulsed arcs at the time of maximum light emission. In a way similar to steady DC arcs, maximal arc diameters ($D_{1\mathrm{Hz}}$, $D_{2\mathrm{Hz}}$ and $D_{5\mathrm{Hz}}$) are approximately proportional to the respective maximal arc current values.

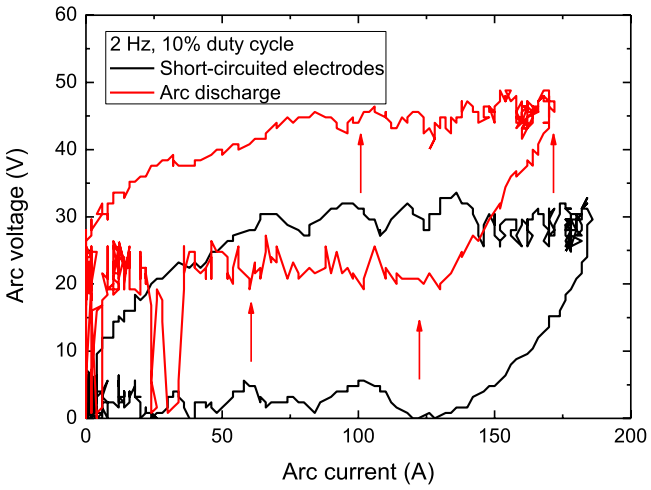

Figure 9. *V–I* characteristics corresponding to one pulse cycle of short-circuited electrodes (black line) and one pulse cycle of arc discharge for separated electrodes (red line) of carbon anode sustained at 2 Hz and 10% duty cycle at 300 Torr pressure. The vertical arrows represent the transition from short-circuit to plasma states. The pulse cycles evolve in time following clockwise rotation on the *V–I* curves.

anode material, χ_i, can be approached by comparing the flux of ejected atoms (calculated from ablation rate) with the flux of ions: the ratio of ion-to-ablation fluxes is a approximately proportional to χ_i, In particular, such ratio and χ_i are identical when an ion beam containing only single ionized atoms is assumed. In all processes, one obtains 0.10–0.35 ratios. However, such ratio reaches unity at the plateau of pulsed arc of carbon anodes. One reason could be the relatively low ablation rate in pulsed arc (10 mg s^{-1} per pulse) compared to the ablation rate in DC full power arc (20 mg s^{-1}). Then, the strong ionization detected in pulsed arcs may owe to an energy-dominated (or material-deficient) scenario, where the unbalance between low ablated material concentration and high power input leads to a substantial ionization degree. In contrast, DC arc discharge ejects atoms at a doubled rate but the electron density is similar to pulsed arcs, so the supplied energy may not suffice for high ionization level and, thus, an important fraction of the ablation flux remains neutral.

4.2. Dynamics in pulsed arcs

The present study shows evidence that the inactive phase in pulsed arcs during regions *i* and *iii* (figure 8), which can be called OFF phase, does show the features of a weak but still burning plasma. Optical glowing on the anode tip during OFF phase was detected in a recent article [10], which is a signature of ignited arc discharge. Interestingly, such anode glowing could be maintained for a few seconds or more by setting $I_{arc} = 0$ ($V_{arc} \approx V_0$). Hence, in pulsed arc processes with frequency range 1–5 Hz and 10% in duty cycle, the system oscillates between a short-living stage of strong, dense arc plasma (ON phase), and a long-living stage of weaker arc plasma (OFF phase). This weak plasma state is identified as the zero-current state found in the present article at arc voltages $\approx V_0$. We refer to such weak plasma stage as zero-current plasma because of the respective very small, negligible arc currents.

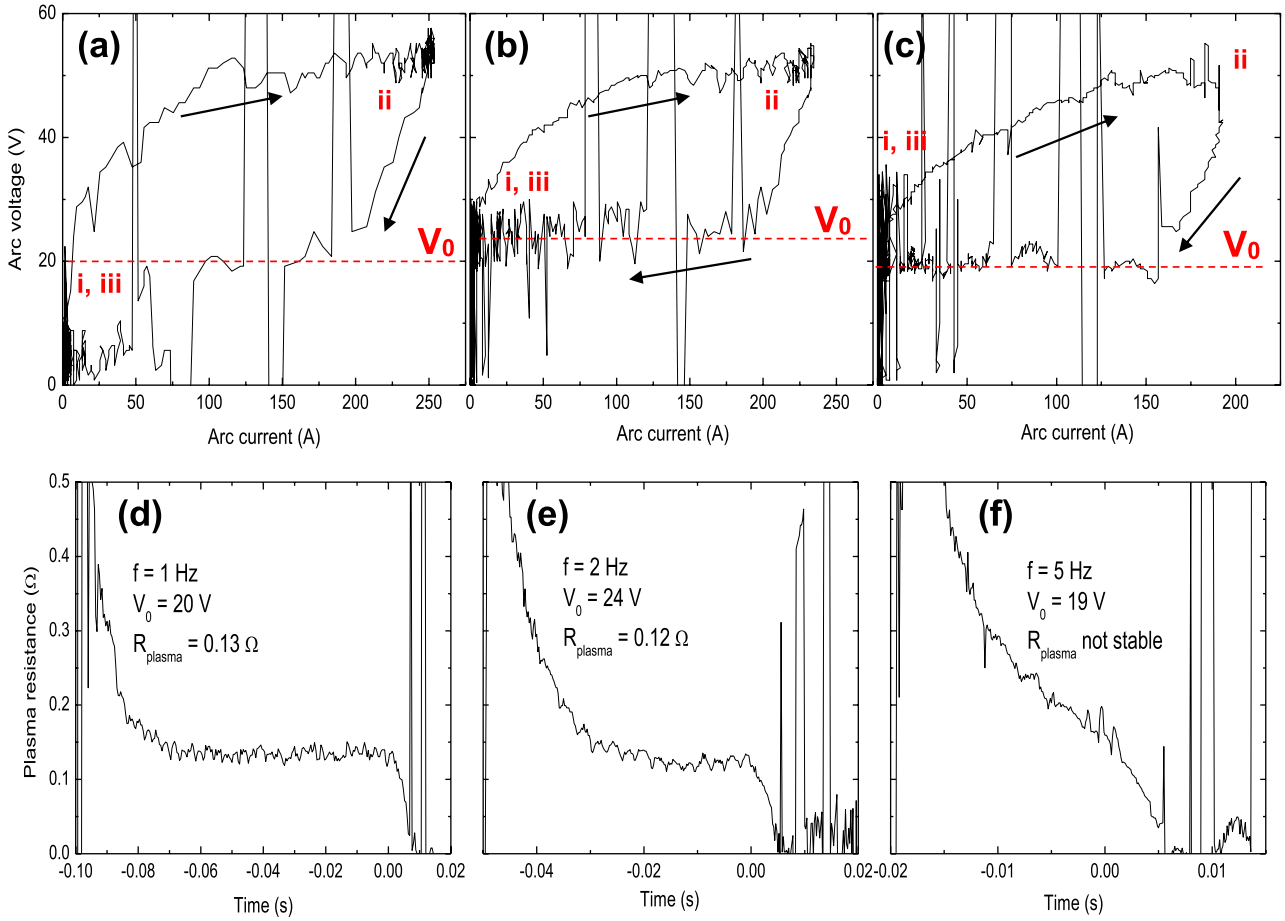

Figure 10. *V–I* characteristics of carbon arc discharges operated at 300 Torr with rectangular pulse signal at (a) 1 Hz; (b) 2 Hz, and (c) 5 Hz. All signals were delivered with a duty cycle of 10%. Arrows indicate the sense of rotation within a pulse cycle. All the characteristics float above the indicated threshold voltage, V_0, which is used as reference to evaluate the plasma arc resistances, $R_{\text{plasma}} = R_{\text{arc}}$, depicted in (d)–(f).

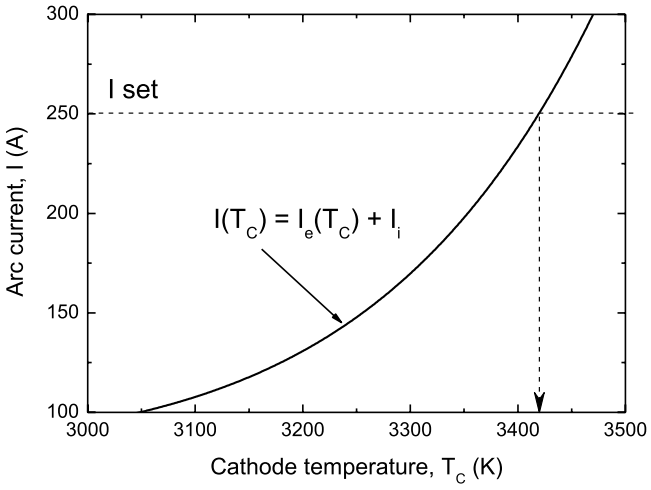

Figure 11. Plot of arc current, I_{arc}, parameterized with the cathode temperature, T_{C}. The value of T_{C} that best fits to the nominal current of 250 A is graphically determined. Electronic current, I_{e}, and ionic current, I_{i}, are computed using equations (5) and (6).

The control of arcs in zero-current state is a relevant topic, as demonstrated by the feasibility of pulsed anodic arc discharge introduced earlier [10], and whose electrical behaviour was explored in section 3.3. Anodic arc plasma volume is basically sustained by thermionic electron emission from cathode and ion generation at the anode sheath. These mechanisms are active during ON phase. The zero-current state at OFF phase requires a potential distribution within gap leading to compensation of electronic current from anode and cathode. For this, both electrodes need to be electron emitters. Hypothetically, thermionic electron emission from anode is compatible with the scenario of transition from positive sheath to negative sheath at the anode. The latter case (negative anode sheath), which has been suggested for atmospheric arc discharge at low current, accounts for electron repulsion from and ion attraction towards anode consistent with a negative voltage drop [16]. Similarly, the existence of a threshold voltage was also found to play a role in the structure of vacuum arcs. There, arc operation down to a critical voltage was indicative of formation of constricted arc characterized by negative anode sheath

Table 2. Data related to electronic and ionic currents in the studied arc discharges.

	Mo DC arc (300 Torr)	Carbon DC arc (300 and 500 Torr)		Carbon pulsed arc (300 Torr)	
Total arc current, I_{arc} (A)	30 A	60 A	150 A	1 Hz, 2 Hz Max. 250 A	5 Hz
Electronic current, I_e (A)	30	55	90	170	—
Ionic current, I_i (A)	<0.5	5	60	80	—
Ion current fraction, I_i/I_{arc}	<0.01	0.08	0.40	0.32	—
Ionic-to-ablated flux ratio	0.15	0.30	0.35	≈ 1	—
Cathode temperature, T_C (K)	3110	3215	3300	3420	—

[15]. Although that study was carried out in the context of low pressure processes, the reported phenomenon could be also connected to the threshold voltage treated in the present paper because constricted arcs are observed in atmospheric arcs as well [23].

In view of the results presented here, one may argue that arc instability near the threshold voltage could be triggered by oscillations between positive and negative anode sheaths, where the voltage drop might be eventually zero. This would diminish ion generation to a great extent. The formation of negative anode sheath is a typical feature in both low-arc current discharges and constricted arcs. As consequence, discharge could tend to vanish near the threshold voltage maybe due to the generation of such instable arc structure. Nevertheless, the fact that electrical breakdown voltage of high-temperature gases is substantially lower than in cold gases might compensate such instability and increase the discharge lifetime [24]. These two competing trends of (1) arc life extension via reduced breakdown voltage, and (2) arc extinction due to anode sheath-induced instability, deserve detailed research in a separate study.

5. Conclusions

Here, we have introduced a circuit model that describes atmospheric arc discharges as a series circuit composed of an equivalent resistor and voltage source. These elements account for the resistances of the arc system (arc column and sheaths) plus a constant voltage which defines a threshold value for arc voltage to keep plasma ignited. This model has been validated by running arc experiments with carbon and Mo anodes and evaluating the circuit parameters using *V–I* curve representation. Hence, steady DC arcs of carbon anodes show sheath resistances around 0.15 Ω and arc column resistances generally one of order of magnitude lower. Similar results were found in pulsed arc discharge at low frequencies (1–5 Hz). These results suggest that most of input power is dissipated at the sheath regions. Values of threshold voltage $V_0 \approx 20$–30 V have been measured in both DC and pulsed arcs, which are consistent with the carbon ionization potential. The hysteresis evidenced in *V–I* plots of pulsed arc cycles has been attributed to an artefact generated by the power supply: this instrument introduces a phase-shift related to the stray inductance of built-in transformer coils. The evaluation of electrical conductivity of plasma column provided an estimate of electron density, which in turn yields to first approximations of electronic and ionic currents of the discharge. Furthermore, the relation between ablated flux and ion flux suggested that pulsed arc discharges are characterized by a high ionization degree. Finally, eventual fluctuations of anode sheath voltage drop around 0 V appearing at arc voltage $V_{arc} \approx V_0$ might explain why working close to the threshold voltage generates arc instabilities leading to discharge extinction. A detailed analysis would require investigation of the anode sheath attachment mode (constricted or diffuse), which is out of the scope of this article.

This study has shown the successful implementation of the circuit model to investigate electric properties of anodic arc processes. The results of this work encourage the transfer and upgrading of this simple model to further anodic arc systems, such as reactive arc discharges and compound/composite anode materials. As concluding remark, it is worth noting that the quantification of electrical parameters in hot arc discharges has been performed self-consistently aside of thermodynamic considerations, thereby assessing the robustness of the circuit model.

Acknowledgments

This work was supported by the US Department of Energy, Office of Science, Fusion Energy Sciences program Award No. DESC0015767, and by the National Science Foundation Grant No. 1747760. The authors thank Dr DB Zolotukhin from George Washington University and Dr Y Raitses from Princeton University for valuable discussions.

ORCID iDs

Carles Corbella https://orcid.org/0000-0002-6201-0680

References

[1] Iijima S 1991 Helical microtubules of graphitic carbon *Nature* **354** 56–8
[2] Arora N and Sharma N N 2014 Arc discharge synthesis of carbon nanotubes: comprehensive review *Diam. Relat. Mater.* **50** 135–50
[3] Shashurin A and Keidar M 2015 Synthesis of 2D materials in arc plasmas *J. Phys. D: Appl. Phys.* **48** 314007
[4] Keidar M and Beilis I I 2018 *Plasma Engineering* 2nd edn (London: Elsevier)

[5] Yeh Y-W, Raitses Y, Koel B E and Yao N 2017 Stable synthesis of few-layered boron nitride nanotubes by anodic arc discharge *Sci. Rep.* **7** 3075
[6] Mansour A R and Hara K 2019 Multispecies plasma fluid simulation for carbon arc discharge *J. Phys. D: Appl. Phys.* **52** 105204
[7] Shashurin A, Keidar M and Beilis I I 2008 Voltage–current characteristics of an anodic arc producing carbon nanotubes *J. Appl. Phys.* **104** 063311
[8] Keidar M and Beilis I I 2009 Modeling of atmospheric-pressure anodic carbon arc producing carbon nanotubes *J. Appl. Phys.* **106** 103304
[9] Palomares J M, Kohut A, Galbács G, Engeln R and Geretovszky Z 2015 A time-resolved imaging and electrical study on a high current atmospheric pressure spark discharge *J. Appl. Phys.* **118** 233305
[10] Corbella C, Portal S, Zolotukhin D B, Martinez L, Lin L, Kundrapu M N and Keidar M 2019 Pulsed anodic arc discharge for the synthesis of carbon nanomaterials *Plasma Sources Sci. Technol.* **28** 045016
[11] Gershman S and Raitses Y 2016 Unstable behavior of anodic arc discharge for synthesis of nanomaterials *J. Phys. D: Appl. Phys.* **49** 345201
[12] Yatom S, Selinsky R S, Koel B E and Raitses Y 2017 'Synthesis-on' and 'synthesis-off' modes of carbon arc operation during synthesis of carbon nanotubes *Carbon* **125** 336–43
[13] He D, Zhao T, Liu Y, Zhu J, Yu G and Ge L 2007 The effect of electric current on the synthesis of single-walled carbon nanotubes by temperature controlled arc discharge *Diam. Relat. Mater.* **16** 1722–6
[14] Fang X, Shashurin A, Teel G and Keidar M 2016 Determining synthesis region of the single wall carbon nanotubes in arc plasma volume *Carbon* **107** 273–80
[15] Keidar M, Schulman M B and Taylor E D 2004 Model of a diffuse column vacuum arc with cathode jets burning in parallel with a high-current plasma column *IEEE Trans. Plasma Sci.* **32** 783–91
[16] Nemchinsky V A and Raitses Y 2016 Anode sheath transition in an anodic arc for synthesis of nanomaterials *Plasma Sources Sci. Technol.* **25** 035003
[17] Raizer Y P 1991 *Gas Discharge Physics* (Berlin: Springer)
[18] Beilis I I 2008 Microplasma generation in a microscale short vacuum arc *Appl. Phys. Lett.* **92** 121501
[19] Lieberman M A and Lichtenberg A J 2005 *Principles of Plasma Discharges and Materials Processing* 2nd edn (Hoboken, NJ: Wiley)
[20] Kundrapu M and Keidar M 2012 Numerical simulation of carbon arc discharge for nanoparticle synthesis *Phys. Plasmas* **19** 073510
[21] Ng J and Raitses Y 2014 Role of the cathode deposit in the carbon arc for the synthesis of nanomaterials *Carbon* **77** 80–8
[22] Yeh Y-W, Raitses Y and Yao N 2016 Structural variations of the cathode deposit in the carbon arc *Carbon* **105** 490–5
[23] Wang C, Sun L, Sun Q, Zhang Z, Xia W and Xia W 2019 Experimental observations of constricted and diffuse anode attachment in a magnetically rotating arc at atmospheric pressure *Plasma Chem. Plasma Process.* **39** 407–21
[24] George D W and Messerle H K 1963 Electrical breakdown in high-temperature gases *Nature* **197** 584–5